Journal of Molecular Structure 1220 (2020) 128556

Contents lists available at ScienceDirect

Journal of Molecular Structure

journal homepage: http://www.elsevier.com/locate/molstruc

Synthesis, thermal, electrochemical and catalytic behavior toward transfer hydrogenation investigations of the half-sandwich Ru^{II} complexes with 2-(2′-quinolyl)benzimidazoles

Ahmet Erdem [a], Rafet Kılınçarslan [a, *], Çiğdem Şahin [a], Osman Dayan [b], Namık Özdemir [c]

[a] Pamukkale University, Faculty of Arts&Sciences, Department of Chemistry, Denizli, 20017, Turkey
[b] Çanakkale Onsekiz Mart University, Faculty of Arts&Sciences, Department of Chemistry, Çanakkale, 17020, Turkey
[c] Ondokuz Mayıs University, Faculty of Education, Department of Mathematics and Science Education, Samsun, 55139, Turkey

ARTICLE INFO

Article history:
Received 2 March 2020
Received in revised form
27 May 2020
Accepted 27 May 2020
Available online 15 June 2020

Keywords:
Hydrogenation
Ru^{II} complexes
Ketones
NN-type ligands
Benzimidazole
Piano-stool complexes

ABSTRACT

A series ligands ($\mathbf{L_{3\text{-}14}}$) of derived from 2-(2′-quinolyl)benzimidazole (QuBim, $\mathbf{L_1}$) and 2-(2′-quinolyl)-5,6-dimethylbenzimidazole (QuDmBim, $\mathbf{L_2}$) which are an *NN*-type ligands have been synthesized and characterized with various techniques such as NMR, UV−vis, FT-IR spectroscopy, elemental analysis and X-ray diffraction. The substituted ligands derived from QuBim and QuDmBim have been used as sustaining ligands in the Ru^{II}-catalyzed transfer hydrogenation (TH) of acetophenone to secondary alcohols in the presence *i*-PrOH/KOH. The half-sandwich complexes ($\mathbf{C_{1\text{-}14}}$) of Ru^{II} with *NN*-type ligands have been synthesized by cleavage of $[(\eta^6\text{-}p\text{-cymene})Ru(\mu\text{-}Cl)]_2$ dimer. The resulting complexes have been characterized by NMR, UV−vis, FT-IR spectroscopy and elemental analysis. The thermal and electrochemical properties of selected complexes and ligands were investigated.

© 2020 Elsevier B.V. All rights reserved.

1. Introduction

In the catalytic reactions, the simplicity of the processes, enabling moderate reaction conditions, high catalytic activity and selectivity make the hydrogen transfer reactions (TH) a preferred way of transferring hydrogen into a system [1]. The extended method used in reducing ketone derivatives to related alcohols is TH reactions. The catalytic TH reactions of ketone are the main and key step for the production of a wide variety of alcohols, including chiral compounds, which are valuable products and precursors for the pharmaceutical, pesticide, flavor, fragrance, material and sensitive chemical industries [2]. In this reaction, the most preferred of 2-propanol; its superior properties such as a source of hydrogen and solvent, reliability, high selectivity, cheapness, accessibility, easy removal of the product resulting from the reaction and environmental friendliness were effective [3]. Besides, TH reactions are equilibrium reactions and the efficiency of the reduction-oxidation pathways are largely dependent on concentration molecule (donor/acceptor) and thermodynamic stability of relevant molecule in equilibrium [4]. These reduction processes, which do not contain molecular hydrogen, deserve a prominent position in the ranks of chemical transformation. It can be envisaged that the application requirements will increase even more for the production of not only synthetic but also fine chemicals.

It attracts the attention of researchers due to the easy binding of nitrogen containing ligands with transition metals, their preparation at high efficiency, the potential of Ru(II) complexes prepared with ligands containing N-donor atoms to increase the catalytic reaction of organic compounds. This property is seen in numerous ruthenium complexes for the hydrogen transfer reaction of ketones as catalyst precursors [5]. The half-sandwich Ru^{II}-(arene) complexes are essential as catalysts such as in alkylation, amination, hydrogenation, hydroformylation and isomerization reactions [6]. The catalyst design provides significant advantages in high yield and selectivity in many catalytic reactions. In particular, ruthenium complexes coordinated with ligands such as NN [7], NNN [8], NO [9], CNN [10] are frequently used in this field. The TH reactions by catalyzed half-sandwich $Ru^{II}(\eta^6\text{-arene})$ complexes which the pioneering work by Noyori and Ikariya et al. [11], have been very attractive subject because of the advantages over classical

* Corresponding author.
E-mail address: rkilincarslan@pau.edu.tr (R. Kılınçarslan).

https://doi.org/10.1016/j.molstruc.2020.128556
0022-2860/© 2020 Elsevier B.V. All rights reserved.

hydrogenation [12] and the trend in these work is dedicated to increase or alter their selectivity, stability and activity by steric and electronic properties. The π-acceptor nitrogen-containing ligands such as *N*-heteroaromatic structure like pyridine- or quinoline-based chelating diamine bidentate ligand 2-(*N*-aromatic structure)-1H-benzimidazoles on ruthenium center in complex have enlarged the scope of TH reactions because of these *NN*-type ligands can be readily derivatized and strongly bonded to metal [3b,7a,13]. In such ligands, the electronic and steric properties on the benzimidazol can be easily modified. Also, this area has attracted increasing interest related to environmentally sustainable processing, simple product separation, and pH dependent selectivity in aqueous medium [14]. For example, the Ru^{II} complexes [(*p*-cymene)Ru(NΛN)$(OH_2)]^{2+}$, [$(\eta^6$-$C_6Me_6)$Ru(phen)Cl]$^+$ and [(*p*-cymene)Ru(NΛN)Cl]$^+$ where NΛN are pyridine-based ligands and phen is 1,10-phenanthroline and other related complexes [3b,15] have been shown to catalyze the reduction of ketones (such as cyclohexanone and acetophenone) to alcohols and imines [16]. The research for TH reactions and efficient catalysts continues to create great interest in ruthenium catalysis. In spite of many efficient the ruthenium complexes based benzimidazole ligands which are biologically effective and medicinally significant compounds [17] have been investigated [3b,7a,18], the availability of metal complexes containing 2-(2′-quinolyl)benzimidazoles remains limited, and only few examples have been published [7a,19].

In this report we expand on previous work involving the use of the half-sandwich Ru^{II} complexes that contain benzyl substituted 2-(2′-quinolyl)benzimidazole ligands and illuminate structural characterization with X-ray diffraction technique (Fig. 1) [7a], we herein report the synthesis of ruthenium complexes, their thermal and electrochemical properties and also their catalytic studies in the catalytic transfer hydrogenation of acetophenone.

2. Experimental

2.1. General considerations

L_1, **L_2** and [$(\eta^6$-*p*-cymene)Ru(μ-Cl)]$_2$ dimer were obtained according to the published procedure in the literature [7a,20]. Information about the devices and techniques used is given in the supporting information section.

2.2. Synthesis of ligands

2.2.1. General procedure for synthesis of 2-(1H-benzimidazol-2-yl) quinoline (***L_1***) and 2-(5,6-dimethyl-1H-benzimidazol-2-yl)quinoline (***L_2***)

Quinaldic acid (20.0 mmol, 3.46 g) and corresponding diamine derivative (20.0 mmol) (*o*-phenylenediamine, 2.163 g or 4,5-dimethyl-*o*-phenylenediamine, 2.724 g) were stirred in polyphosphoric acid (PPA) (40 mL) for 4h at 200 °C under argon. At the end this time, the green-colored molten fluid was poured into iced water. Then the ammonium hydroxide was added to make the pH: 9 and obtaining solid was filtered off. The precipitate was boiled with EtOH for 2h with activated charcoal. Finally, the product was recrystallized by EtOH. For characterization data **L_1** and **L_2**, please see supporting materials.

2.2.2. General procedure for the synthesis of other N^N-type ligands (***$L_{3\text{-}14}$***)

L_3-L_8 ligands were synthesized starting from **L_1** while **L_9-L_{14}** ligands were synthesized starting from **L_2** by modification of the literature procedure [7a,21]. **L_1** (10.0 mmol, 2.45 g) or **L_2** (10.0 mmol, 0.27 g) and KOH (10.0 mmol, 0.56 g) were stirred in a Schlenk tube at 40 °C for 2h in PhMe. At the end of the time, the corresponding benzyl halide derivative (11.0 mmol) (benzyl bromide, 1.92 g; 2-methylbenzyl chloride, 1.56 g; 2,4,6-trimethylbenzyl chloride, 1.86 g; 2,3,5,6-tetramethylbenzyl chloride, 2.01 g; 2,3,4,5,6-pentamethylbenzyl chloride, 2.16 g; 1-(chloromethyl) naphthalene, 2.00 g) was added to the reaction mixture and the mixture was refluxed for 8h. The solvent was removed in vacuo, and the residue was filtered by adding CH_2Cl_2. The filtrate was allowed to crystallize by adding hexane. For characterization data **L_3-L_{14}**, please see supporting materials.

2.3. General procedure for the synthesis of [RuCl($L_{1\text{-}14}$)(η^6- *p*-cymene)]Cl ($C_{1\text{-}14}$)

The ligands (1.0 mmol) and [$RuCl_2$(*p*-cymene)]$_2$ (0.5 mmol) were refluxed in ethanol for 8 h. At the end of this time, the mixture was cooled at room temperature. The solvent was evaporated to some extent. Then, the mixture was precipitated by addition of diethyl ether. The precipitate was filtered off, washed and dried. The product was recrystallized from EtOH/Et_2O.

2.4. X-ray crystallography

Intensity data of the compounds were collected with a STOE IPDS II diffractometer at room temperature using graphite-monochromated Mo Kα radiation by applying the ω-scan method. Data collection and cell refinement were carried out using X-AREA [22] while data reduction was applied using X-RED32 [22]. The structure solutions were obtained using SIR2019 [23] and SHELXL-2018 [24] was applied for the refinements. The coordinates of the water H atom were determined from a difference Fourier map and refined freely [O—H = 0.85(4)-0.88(3) Å]. The remaining H atoms were inserted in idealized positions and treated using a riding model, fixing the bond lengths at 0.86, 0.93, 0.97 and 0.96 Å for NH, CH, CH_2 and CH_3 atoms, respectively. The displacement parameters of the H atoms were fixed at $U_{iso}(H) = 1.2U_{eq}$ ($1.5U_{eq}$ for CH_3). The crystallographic data and refinement parameters are summarized in Table 1. OLEX2 [25] was used to prepare artwork representations.

3. Results and discussions

3.1. Synthesis and characterization of compounds

2-(1H-benzimidazol-2-yl)quinoline (**L_1**, **QuBim**) [20] and 2-(5,6-dimethyl-1H-benzimidazol-2-yl)quinoline (**L_2**, **QuDmBim**) [26] substances also used as chelating ligands were synthesized in

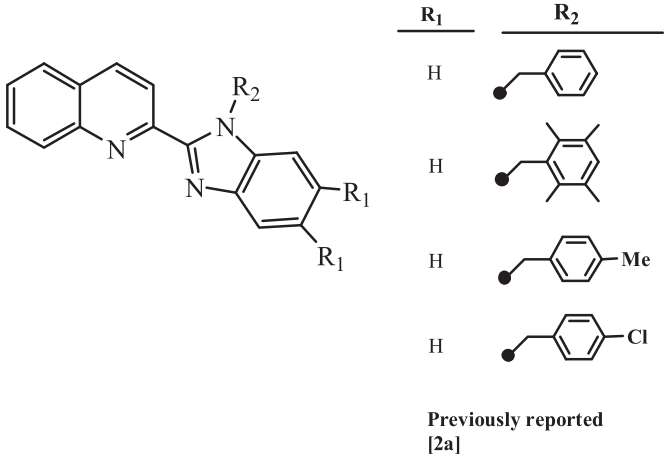

Fig. 1. The quinoline based ligands synthesized in the previous study.

Table 1
Crystal data and structure refinement parameters for **L_2**, **L_4**, **L_{12}** and **L_{14}**.

Parameters	L_2	L_4	L_{12}	L_{16}
CCDC depository	1966794	1966795	1966796	1966797
Color/shape	Colorless/prism	Colorless/prism	Colorless/prism	Colorless/prism
Chemical formula	$C_{18}H_{15}N_3 \cdot H_2O$	$C_{24}H_{19}N_3$	$C_{29}H_{29}N_3$	$C_{29}H_{23}N_3$
Formula weight	291.34	349.42	419.55	413.50
Temperature (K)	296(2)	296(2)	296(2)	296(2)
Wavelength (Å)	0.71073 Mo Kα	0.71073 Mo Kα	0.71073 Mo Kα	0.71073 Mo Kα
Crystal system	Triclinic	Monoclinic	Monoclinic	Monoclinic
Space group	$P\bar{1}$ (No. 2)	$P2_1/c$ (No. 14)	$P2_1/n$ (No. 14)	$P2_1/c$ (No. 14)
Unit cell parameters				
a, b, c (Å)	7.5663(7), 8.9530(8), 11.9952(12)	14.2337(8), 8.9912(5), 14.8750(10)	9.1696(5), 21.0565(12), 12.8657(7)	18.0898(17), 6.2515(5), 19.231(2)
α, β, γ (°)	92.314(8), 93.957(8), 111.075(7)	90, 101.114(5), 90	90, 106.767(4), 90	90, 92.262(8), 90
Volume (Å^3)	754.55(13)	1868.0(2)	2378.5(2)	2173.1(4)
Z	2	4	4	4
$D_{calc.}$ (g/cm^3)	1.282	1.242	1.172	1.264
μ (mm^{-1})	0.082	0.074	0.069	0.075
Absorption correction	Integration	Integration	Integration	Integration
$T_{min.}, T_{max.}$	0.9661, 0.9936	0.9552, 0.9809	0.9628, 0.9851	0.9719, 0.9965
F_{000}	308	736	896	872
Crystal size (mm^3)	0.66 × 0.15 × 0.09	0.79 × 0.56 × 0.25	0.74 × 0.38 × 0.19	0.64 × 0.13 × 0.03
Diffractometer	STOE IPDS II	STOE IPDS II	STOE IPDS II	STOE IPDS II
Measurement method	ω scan	ω scan	ω scan	ω scan
Index ranges	$-9 \le h \le 9, -11 \le k \le 11, -15 \le l \le 15$	$-18 \le h \le 17, -11 \le k \le 10, -19 \le l \le 19$	$-11 \le h \le 11, -27 \le k \le 27, -15 \le l \le 16$	$-21 \le h \le 21, -7 \le k \le 7, -22 \le l \le 22$
θ range for data collection (°)	$2.881 \le \theta \le 27.551$	$2.661 \le \theta \le 27.724$	$1.915 \le \theta \le 27.726$	$2.120 \le \theta \le 25.048$
Reflections collected	16965	12415	15807	12871
Independent/observed reflections	3478/1795	4368/1978	5552/2267	3851/1509
$R_{int.}$	0.0752	0.0554	0.0723	0.1619
Refinement method	Full-matrix least-squares on F^2	Full-matrix least-squares on F^2	Full-matrix least-squares on F^2	Full-matrix least-squares on F^2
Data/restraints/parameters	3478/0/209	4368/0/245	5552/0/295	3851/0/291
Goodness-of-fit on F^2	0.967	0.870	0.856	0.964
Final R indices [$I > 2\sigma(I)$]	$R_1 = 0.0595$, w$R_2 = 0.0963$	$R_1 = 0.0471$, w$R_2 = 0.0920$	$R_1 = 0.0536$, w$R_2 = 0.0936$	$R_1 = 0.0852$, w$R_2 = 0.0720$
R indices (all data)	$R_1 = 0.1373$, w$R_2 = 0.1146$	$R_1 = 0.1240$, w$R_2 = 0.1132$	$R_1 = 0.1615$, w$R_2 = 0.1208$	$R_1 = 0.2184$, w$R_2 = 0.0953$
$\Delta\rho_{max.}, \Delta\rho_{min.}$ (e/Å^3)	0.13, −0.16	0.12, −0.12	0.11, −0.14	0.12, −0.12

moderate to high yield in a single step from commerically available quinaldic acid and corresponding diamine derivative *o*-phenylenediamine or 4,5-dimethyl-*o*-phenylenediamine in polyphosphoric acid (PPA), respectively. **$L_{3\text{-}14}$** ligands (N^N-type) which are *N*-substitution products were synthesized in alkaline solution with various benzylhalide derivatives (Scheme 1). The compounds, **L_3** and **L_6** of the *N*-substituted products were previously synthesized by Dayan et al. (Fig. 1) [7a]. The NMR characterization data of **$L_{1\text{-}3}$** and **L_6** compounds matched those reported in the literature. Other ligands and ruthenium complexes synthesized from them are new in the literature. The half-sandwich Ru(II) complexes (**$C_{1\text{-}14}$**) corresponding to **$L_{1\text{-}14}$** ligands were synthesized from a 2:1

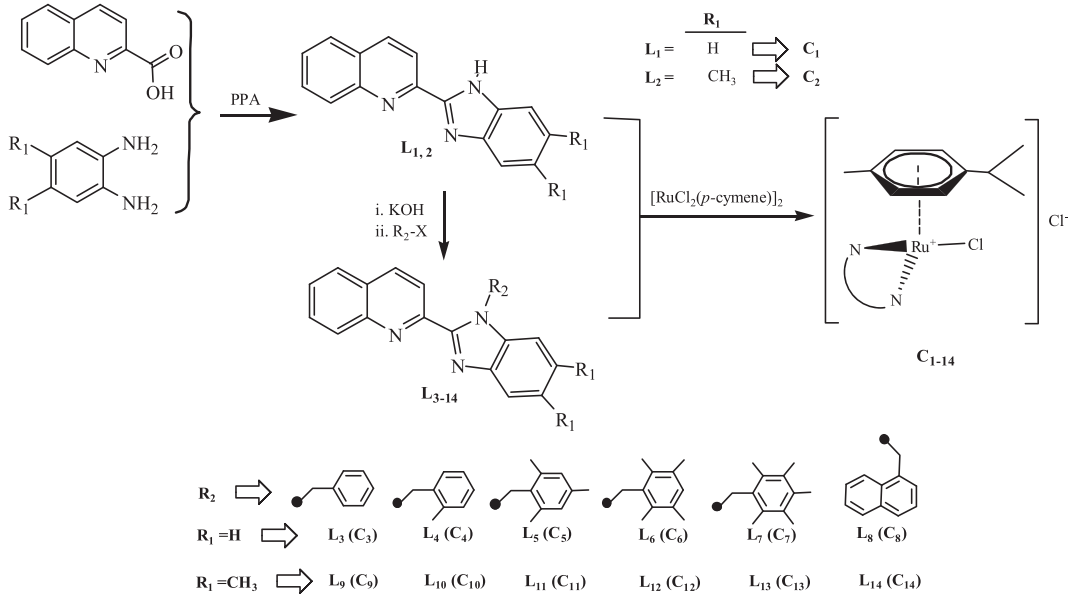

Scheme 1. Synthesis of ligands and Ru(II) complexes.

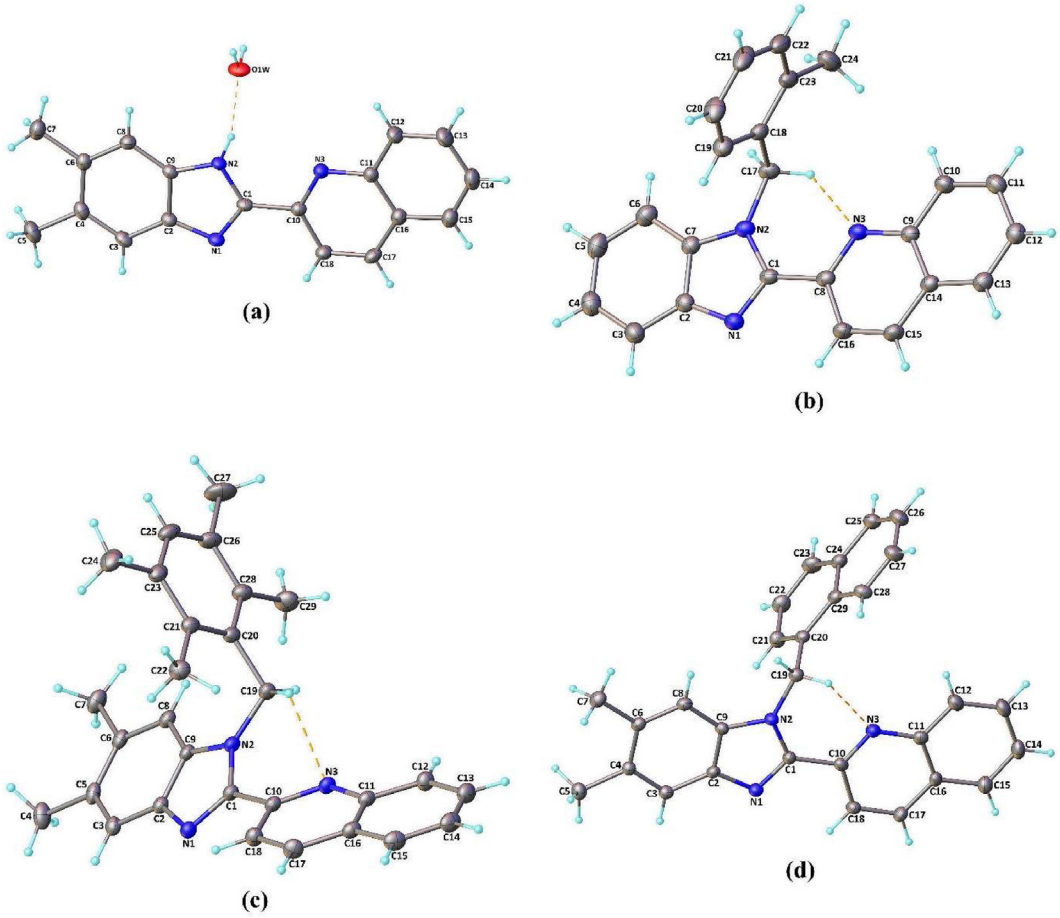

Fig. 2. Molecular structures of $\mathbf{L_2}$ **(a)**, $\mathbf{L_4}$ **(b)**, $\mathbf{L_{12}}$ **(c)** and $\mathbf{L_{14}}$ **(d)**, showing the atom numbering schemes. H atoms are shown as small spheres of arbitrary radii and the intra- or intermolecular interactions are represented by dashed lines.

mixture of ligand and $[RuCl_2(p\text{-cymene})]_2$ in ethanol and were isolated in high yields. All analyzes including NMR data (^1H and ^{13}C) are presented in the supporting information. Furthermore, the solid-state structures of $\mathbf{L_2}$, $\mathbf{L_4}$, $\mathbf{L_{12}}$ and $\mathbf{L_{14}}$ were determined by single crystal X-ray diffraction. However, we tried to obtain the complex crystal for the X-ray difraction studies, but we could not obtain a suitable crystal. $\mathbf{L_{1\text{-}14}}$ and $\mathbf{C_{1\text{-}14}}$ compounds were soluble in commonly used solvents such as MeOH, EtOH, DMF, DMSO and CH_2Cl_2.

Table 2
Selected geometric parameters for $\mathbf{L_2}$, $\mathbf{L_4}$, $\mathbf{L_{12}}$ and $\mathbf{L_{14}}$.

Parameters	L_2	L_4	L_{12}	L_{14}
Bond lengths (Å)				
N1−C1	1.323(2)	1.316(2)	1.311(3)	1.320(5)
N1−C2	1.386(3)	1.381(2)	1.385(3)	1.387(5)
N2−C1	1.356(2)	1.3796(19)	1.379(3)	1.376(5)
N2−C7	-	1.377(2)	-	-
N2−C9	1.375(3)	-	1.381(3)	1.395(5)
N2−C17	-	1.4584(19)	-	-
N2−C19	-	-	1.461(3)	1.468(5)
Bond angles (°)				
N1−C1−N2	112.48(19)	112.16(16)	113.84(18)	114.0(4)
C1−N1−C2	105.04(16)	105.60(14)	104.24(18)	104.0(4)
C1−N2−C7	-	106.35(13)	-	-
C1−N2−C9	107.46(16)	-	105.28(18)	105.2(4)
C1−N2−C17	-	129.22(16)	-	-
C1−N2−C19	-	-	128.31(18)	129.6(4)
C7−N2−C17	-	124.41(14)	-	-
C9−N2−C19	-	-	125.87(17)	124.9(4)
N1−C1−C8	-	122.17(14)	-	-
N1−C1−C10	124.71(17)	-	121.95(19)	121.2(4)
N2−C1−C8	-	125.63(14)	-	-
N2−C1−C10	122.81(17)	-	124.2(2)	124.8(4)
N2−C17−C18	-	113.78(13)	-	-
N2−C19−C20	-	-	114.04(18)	113.8(4)

The NH peaks in QuBim ($\mathbf{L_1}$) and QuDmBim ($\mathbf{L_2}$) were appeared a signals at δ 13.25 and δ 13.0 ppm as a broad singlet in the ^1H NMR spectra of compounds, respectively. The aromatic protons of QuBim ($\mathbf{L_1}$) compound in the spectra, along with signals due to the two aromatic fragments which are benzimidazol and quinoline moiety, in the region of δ 7.25−7.61 and δ 7.81−8.49 ppm were seen, while QuDmBim ($\mathbf{L_2}$) was seen in the range of δ 7.39−7.51 and δ 7.51−8.44 ppm, respectively. In addition, the methyl protons in the benzimidazol skeleton in QuDmBim ($\mathbf{L_2}$) were seen at δ 2.29 ppm. The main difference that separates the ^1H NMR spectra $\mathbf{L_{3\text{-}14}}$ which are *N*-substitution products from $\mathbf{L_1}$ and $\mathbf{L_2}$ is loss of the NH proton in the benzimidazol fragment and formation of new peaks of benzylic CH_2 protons. The benzylic CH_2 protons were observed as singlet peaks around δ 6.18−6.48 ppm in $\mathbf{L_{3\text{-}14}}$ compounds. In addition, the aromatic protons belonging to benzylic groups in compounds $\mathbf{L_{3\text{-}14}}$ were monitored around δ 6.25−8.55 ppm.

The main difference of half-sandwich Ru(II) complexes ($\mathbf{C_{1\text{-}14}}$) from ligands ($\mathbf{L_{1\text{-}14}}$) is the emergence of new peaks belonging to *p*-cymene groups in the ^1H NMR spectra. The ruthenium complexes, $\mathbf{C_1}$ and $\mathbf{C_2}$ synthesized from the non-*N*-substituted ligands, $\mathbf{L_1}$ and $\mathbf{L_2}$, of which complex, $\mathbf{C_2}$ is novel. The protons of *p*-cymene groups of $\mathbf{C_1}$ and $\mathbf{C_2}$ were observed as doublet of doublets at δ 0.72 ppm and

δ 0.65 ppm belonging to CH_3 in isopropyl group, as multiplet δ 2.18–2.25 ppm and δ 2.07–2.18 ppm belonging to CH in isopropyl group, as singlet at δ 2.30 ppm belonging to CH_3 the same for both complexes, as doublets at δ 6.13, 6.27, 6.34 (dd) ppm and δ 6.05, 6.20, 6.27, 6.36 ppm belonging to aromatic CH, respectively. It is thought that some unusual peaks are seen due to complex symmetry in ^{1}H NMR spectra for **C$_1$** and **C$_2$**. This is also supported by ^{13}C NMR spectra and there are six peaks some of which doublets for aromatic CH and CH_3 in isopropyl group. The protons in benzimidazole and quinoline skeletons of **L$_1$** and **L$_2$** were observed to generally shifted downfield after complexation. In the ^{1}H NMR spectra of C_2, the peak of the NH proton in the structure was not observed as in the **C$_1$** complex [7a]. This situation can be explained by the fact that **C$_1$** and **C$_2$** have an ionic character. After all these determinations, when looking at other the half-sandwich Ru(II) complexes (**C$_{3\text{-}14}$**), ^{1}H NMR spectra were more complicated due to the excess of aromatic protons. Besides, similar slopes are also observed ^{1}H and ^{13}C NMR spectra of **C$_{3\text{-}8}$** and **C$_{9\text{-}14}$** complex series. The larger data can be found in the supporting information for all compounds.

The ESI-MS chromatograms of **C$_2$**, **C$_8$**, **C$_{10}$** and **C$_{14}$** ionic complexes are given in the supporting information section. In the mass spectra of **C$_2$** complex consisting of 2-(5,6-dimethyl-1H-benzimidazol-2-yl)quinoline (**L$_2$**) ligand and auxiliary ligands (Cl and *p*-cymene), mass fragmentation was the result of separation of the Cl group that remained outside the coordination sphere $[M\text{-}Cl]^+$ peak was observed at 544.28. Similarly, $[M\text{-}Cl]^+$ peaks for other complexes (**C$_8$**, **C$_{10}$** and **C$_{14}$**) were observed in high abundance at 656.218, 648.38 and 684.39, respectively. In addition, lower abundances of $[M^+ + 2H]$ and $[M + Cl]$ peaks were observed in all the mentioned complexes.

The NH and C=N streching vibration bands were determined at 3484 and 1618 cm^{-1} for **L$_1$**, at 3495 and 1617 cm^{-1} for **L$_2$**, respectively. The main differences of **L$_{3\text{-}14}$** from **L$_1$** and **L$_2$** used as starting materials are loss of the NH band and the presence of aliphatic stretching bands relation to CH_2 in benzylic group between 2962 and 3017 cm^{-1}. The C=N streching vibration bands of **L$_3$-L$_{14}$** were observed at the region of 1611–1618 cm^{-1}. In addition to the observation of the new peaks of the *p*-cymene group after the formation of the half-sandwich Ru(II) complexes (**C$_{1\text{-}14}$**), the C=N stretching vibration bands shifted slightly compared to ligands (1618 cm^{-1} for **C$_1$**, 1617 cm^{-1} for **C$_2$**, 1614 cm^{-1} for **C$_3$**, 1615 cm^{-1} for **C$_4$**, 1616 cm^{-1} for **C$_5$**, 1618 cm^{-1} for **C$_6$**, 1620 cm^{-1} for **C$_7$**, 1617 cm^{-1} for **C$_8$**, 1620 cm^{-1} for **C$_9$**, 1622 cm^{-1} for **C$_{10}$**, 1620 cm^{-1} for **C$_{11}$**, 1621 cm^{-1} for **C$_{12}$**, 1620 cm^{-1} for **C$_{13}$**, 1622 cm^{-1} for **C$_{14}$**). In the FT-IR spectra of Ru(II) complexes, $C_{1\text{-}14}$, were also seen broad band in the range of about 3300–3450 cm^{-1} relation to strecthing bands from water molecules. The half-sandwich Ru(II) complexes in solid form have partially hyrgroscopic properties. In UV–Vis spectra of QuBim(**L$_1$**), QuDmBim(**L$_2$**) and derived from them the other ligands (**L$_{3\text{-}14}$**), the peaks belonging to $\pi \rightarrow \pi^*$ and $n \rightarrow \pi^*$ transitions were monitored around 306–361 nm. This transitions are red-shifted with the complexation and new charge transfer band belonging **Ru(π)$\rightarrow$ dπ^*** CT occurred around 373–389 nm.

3.2. Description of the crystal structures

The structures of the **L$_2$**, **L$_4$**, **L$_{12}$** and **L$_{14}$** ligands were obtained by SXRD studies. The molecular diagrams of **L$_2$**, **L$_4$**, **L$_{12}$** and **L$_{14}$** with the atom-numbering scheme are depicted in Fig. 2, while important bond distances and angles are listed in Table 2 in the supporting information section.

The planes of the benzimidazole and the quinoline, being linked by *ortho* carbon atoms, are almost coplanar with a dihedral angle of 3.36(7)° in **L$_2$**, 4.77(6)° in **L$_4$** and 3.04(13)° in **L$_{14}$**. whilst these planes are inclined at an angle of 33.77(7)° in **L$_{12}$**. In addition, the benzene ring in **L$_4$** and **L$_{12}$** and the naphthalene ring in **L$_{14}$** make dihedral angles of 89.53(9) and 85.71(8)° in **L$_4$**, 83.25(7) and 61.85(7)° in **L$_{12}$** and 85.46(14) and 88.42(15)° in **L$_{14}$** with the benzimidazole and the quinoline ring planes, respectively. Although the N1–C1 bond is slightly longer than the typical imino C=N bond, the bond lengths and angles are standard [27] and agree well with the literature values [7a,26,28-32]. In all compounds, imine nitrogen atoms of benzimidazole and quinoline moieties are placed in *trans* position. This very likely reduces electrostatic interaction of the lone pairs of the imine nitrogen atoms and also serves to prevent a steric clash of the H atom at the 3-position of the quinoline ring with the amino or methylene H atom at the 1-position of the benzimidazole ring [31].

In the molecular structure of **L$_2$**, no intramolecular interactions exist. In the crystal structure of **L$_2$**, the benzimidazole-quinoline molecule is linked to water molecule by means of an N–H···O

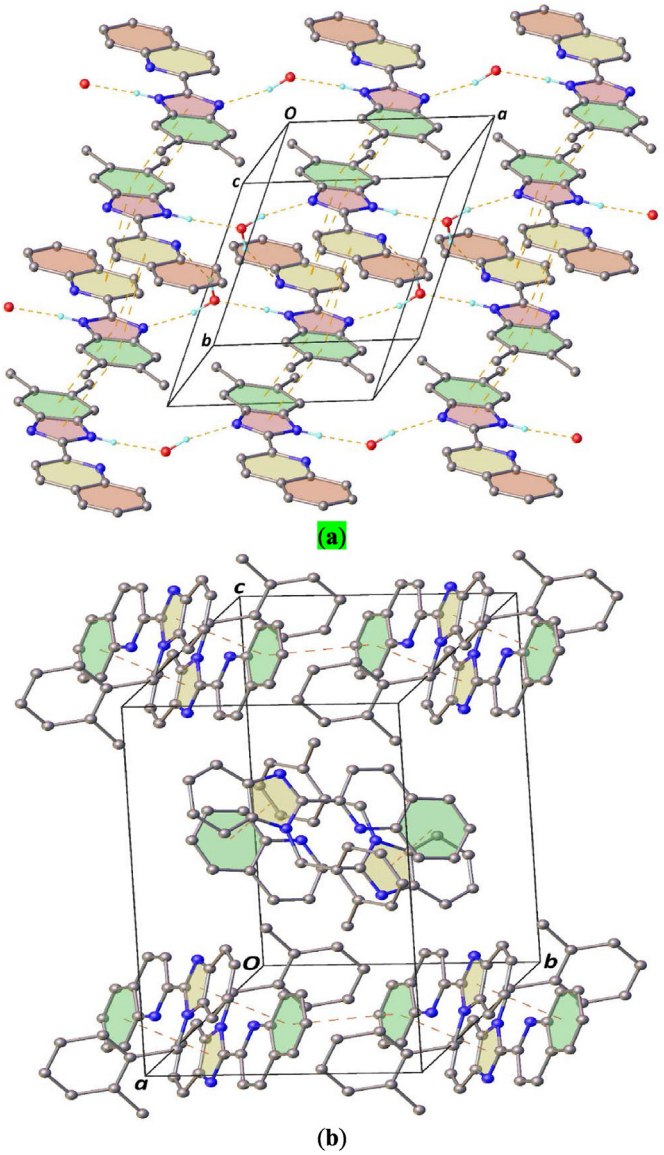

Fig. 3. (**a**) Part of the crystal structure of **L$_2$**, showing the intermolecular interactions as dashed lines. For the sake of clarity, H atoms not involved in the interactions shown have been omitted, (**b**) Part of the crystal structure of **L$_4$**, showing the intermolecular interactions as dashed lines. For the sake of clarity, H atoms have been omitted.

hydrogen bond, while the water molecule is linked it *via* two O—H···N interactions. There are also face-to-face π···π stacking interactions in which the interplanar distances between benzimidazole and quinoline rings are in the range 3.6388(14)-3.8714(15) Å (Fig. 3a, in the supporting information section). In the molecular structures of **L_4**, **L_{12}** and **L_{14}**, an intramolecular C—H···N contact leads to the formation of six-membered ring with graph-set descriptor *S*(6) [33]. In the crystal structure of **L_4** and **L_{12}**, no classic hydrogen bonds are found. Instead, there are face-to-face π···π stacking interactions (Figs. 3b and 4a, in the supporting information section) in which the interplanar distances between benzimidazole and quinoline rings change from 3.6264(12) to 3.7023(11) Å in **L_4** and the interplanar distances between benzimidazole rings range from 3.7812(16) to 3.9035(15) Å in **L_4**. In the case of **L_{14}**, neither classic hydrogen bonds nor other weak interactions are observed. As a result, van der Waals interactions stabilize the molecular packing (Fig. 4b, in the supporting information section). Full details of the hydrogen-bonding geometry are given in Table 3 in the supporting information section.

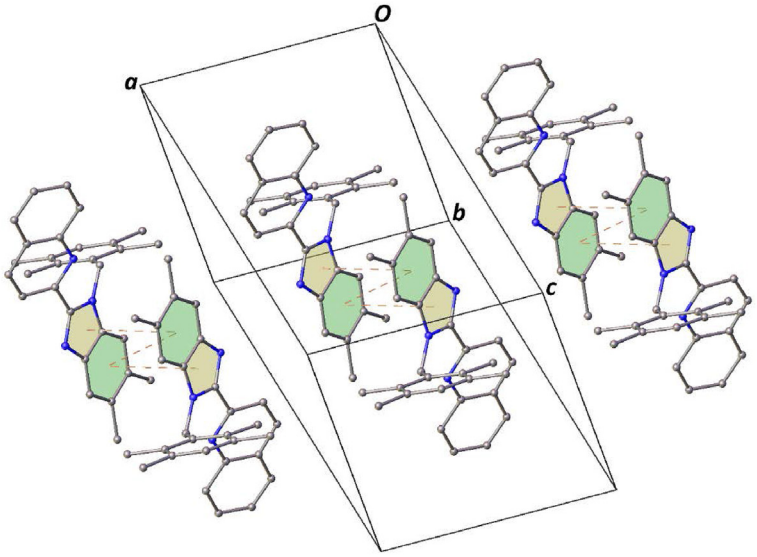

(a)

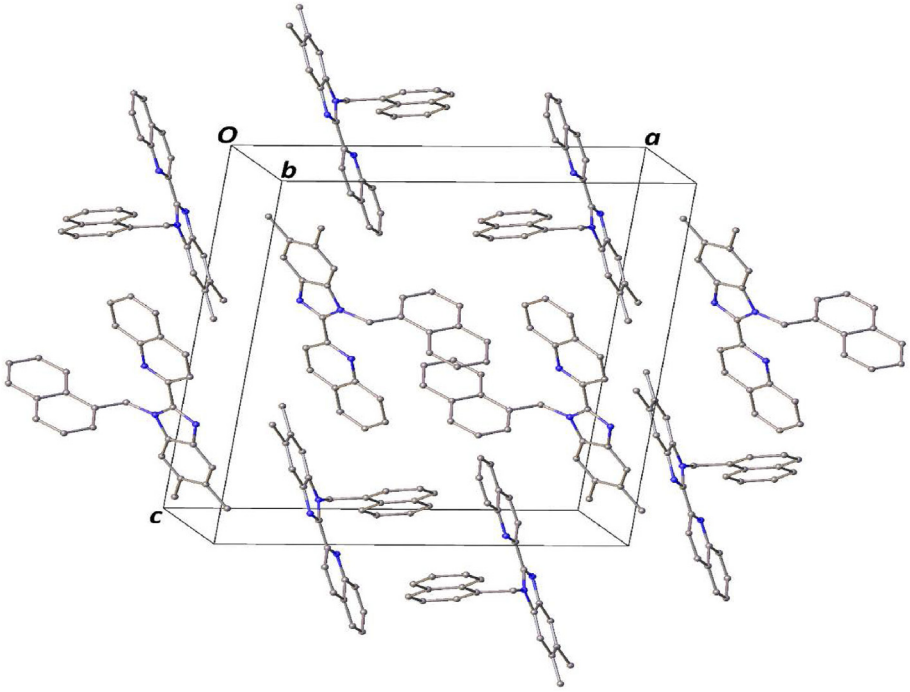

(b)

Fig. 4. (**a**) Part of the crystal structure of **L_{12}**, showing the intermolecular interactions as dashed lines. For the sake of clarity, H atoms have been omitted, (**b**) Part of the crystal structure of **L_{14}**. For the sake of clarity, H atoms have been omitted.

Table 3
Hydrogen bonding geometry for $\mathbf{L_2}$, $\mathbf{L_4}$, $\mathbf{L_{12}}$ and $\mathbf{L_{14}}$.

D—H···A	D—H (Å)	H···A (Å)	D···A (Å)	D—H···A (°)
L_2				
O1W—H1A···N1^{i}	0.88(3)	1.96(3)	2.816(2)	164(3)
N2—H2···O1W	0.86	1.95	2.786(2)	163
O1W—H1B···N3^{ii}	0.85(4)	2.28(4)	3.044(3)	150(3)
L_4				
C17—H17B···N3	0.97	2.36	2.882(2)	113
L_{12}				
C19—H19B···N3	0.97	2.40	3.013(3)	121
L_{14}				
C19—H19A···N3	0.97	2.38	2.882(6)	112

Symmetry codes: ^{i} $x+1, y, z$; ^{ii} $-x+2, -y+1, -z+1$; ^{iii} $x+1, y, z$.

3.3. The thermal behavior of the ruthenium complexes

The TGA curves of the ruthenium complexes ($\mathbf{C_{1\text{-}14}}$) were obtained at heating rate of 20 °C/min in the temperature range of 50—1000 °C under N_2 atmosphere. The thermoanalytical data of the complexes are summarized in Table 4. TGA curves of some selected complexes are given in Fig. 5. The TGA curves of the complexes show decomposition temperatures above 200 °C. In the TGA curves of $\mathbf{C_1}$ and $\mathbf{C_2}$, the first mass loss in the range 50—387 °C is attributed to the quinoline fragment of $\mathbf{L_1}$ (or $\mathbf{L_2}$). In the second step, the benzimidazole fragment of $\mathbf{L_1}$ (or $\mathbf{L_2}$) ligand and cymene ligand of $\mathbf{C_1}$ (or $\mathbf{C_2}$) complex undergoes decomposition in the temperature range 326—1000 °C. The complex exhibits a residue above 1000 °C, corresponding two chloride and ruthenium. Thermal behaviors of $\mathbf{C_3}$ and $\mathbf{C_4}$ display two decomposition steps which give lower thermal stability in the presence of the benzyl groups on benzimidazole of $\mathbf{L_3}$ (or $\mathbf{L_4}$) ligand. In the first step, the mass loss of the complexes $\mathbf{C_3}$ and $\mathbf{C_4}$ (32.52—33.25%) were observed due to the elimination of the benzimidazole with benzyl moiety for $\mathbf{C_3}$ and methyl groups on benzyl moiety for $\mathbf{C_4}$. Finally, mass loss (28.98—29.36%) of complexes in the temperature range 338—1000 °C shows the removal of the quinoline group of ligand and alkyl groups (CH_3+ $CH(CH_3)_2$) of cymene. After this decomposition step, the mass loss is around 62% up to 1000 °C. The residue with the mass 37.77—38.12% may be assigned to benzene ring, two chloride and ruthenium. The decomposition temperature ranges and the percentage of mass loss of the complexes ($\mathbf{C_1}$-$\mathbf{C_{10}}$, $\mathbf{C_{12}}$-$\mathbf{C_{14}}$) are given in Table 4. The obtained results indicate that the synthesized complexes have high thermal stability required for catalyst applications.

3.4. Electrochemical data

The cyclic voltammograms of the complexes ($\mathbf{C_1}$, $\mathbf{C_2}$, $\mathbf{C_8}$ and $\mathbf{C_{14}}$) show one oxidation at around 1.27 V (Fig. 6a). The extent of the oxidation peak can be attributed to the contribution of ruthenium metal as the main character and *p*-cymene to the highest occupied

Table 4
Mass loss (%) of the ruthenium(II) complexes ($\mathbf{C_{1\text{-}14}}$) in the different temperature ranges.

Complex	TGA Temp. range (°C)	Mass loss (%)		Decomposition product loss
		Found	Calc.	
C1	50—326	23.43	23.24	C_9H_6N
	326—1000	45.34	45.58	$C_7H_5N_2$+CH_3+C_6H_4+$CH(CH_3)_2$
	>1000	31.23	31.18	2Cl+Ru
C2	50—387	22.02	22.11	C_9H_6N
	387—1000	48.20	48.21	2CH_3+$C_7H_3N_2$+CH_3+C_6H_4+$CH(CH_3)_2$
	>1000	29.78	29.68	2Cl+Ru
C3	50—396	32.52	32.30	$C_7H_4N_2$-CH_2-C_6H_5
	396—1000	29.36	29.03	C_9H_6N+CH_3+$CH(CH_3)_2$
	>1000	38.12	38.67	C_6H_4+2Cl+Ru
C4	50—338	33.25	33.75	$C_7H_4N_2$-CH_2-C_6H_4+CH_3
	338—1000	28.98	28.41	C_9H_6N+CH_3+$CH(CH_3)_2$
	>1000	37.77	37.84	C_6H_4+2Cl+Ru
C5	50—400	36.49	36.47	$C_7H_4N_2$-CH_2-C_6H_2+3CH_3
	400—1000	32.18	32.43	C_9H_7N+CH_3+$CH(CH_3)_2$+Cl
	>1000	31.33	31.10	C_6H_4+Cl+Ru
C6	50—379	37.29	37.74	$C_7H_4N_2$-CH_2-C_6H_1+4CH_3
	379—1000	31.08	31.93	C_9H_6N+CH_3+$CH(CH_3)_2$+Cl
	>1000	31.63	30.33	C_6H_4+Cl+Ru
C7	53—385	38.77	38.97	$C_7H_4N_2$-CH_2-C_6H_0+5CH_3
	385—1000	31.73	31.30	C_9H_6N+CH_3+$CH(CH_3)_2$+Cl
	>1000	29.50	29.87	C_6H_4+Cl+Ru
C8	50—531	37.21	37.20	$C_7H_4N_2$-CH_2-$C_{10}H_7$
	531—1000	32.43	32.06	C_9H_6N+CH_3+$CH(CH_3)_2$+Cl
	>1000	30.36	30.74	C_6H_4+Cl+Ru
C9	50—340	19.18	19.14	C_9H_6N
	340—1000	60.18	60.47	2CH_3+$C_7H_3N_2$-CH_2-C_6H_5 +CH_3+C_6H_4+$CH(CH_3)_2$+Cl
	>1000	20.64	20.39	Cl+Ru
C10	50—314	18.79	18.74	C_9H_6N
	314—1000	61.83	61.29	2CH_3+$C_7H_3N_2$-CH_2-C_6H_4+CH_3+CH_3+C_6H_4+$CH(CH_3)_2$+Cl
	>1000	19.38	19.97	Cl+Ru
C12	50—317	17.41	17.66	C_9H_6N
	317—1000	63.98	63.53	2CH_3+$C_7H_2N_2$-CH_2-C_6H_0+4CH_3+CH_3+C_6H_4+$CH(CH_3)_2$+Cl
	>1000	18.61	18.81	Cl+Ru
C13	50—353	17.47	17.32	C_9H_6N
	353—1000	64.25	64.23	2CH_3+$C_7H_2N_2$-CH_2-C_6H_0+5CH_3+CH_3+C_6H_4+$CH(CH_3)_2$+Cl
	>1000	18.28	18.45	Cl+Ru
C14	50—488	39.40	39.65	2CH_3+$C_7H_2N_2$-CH_2-$C_{10}H_7$
	488—1000	36.54	36.44	C_9H_6N+CH_3+C_6H_4+$CH(CH_3)_2$
	>1000	24.06	23.91	2Cl+Ru

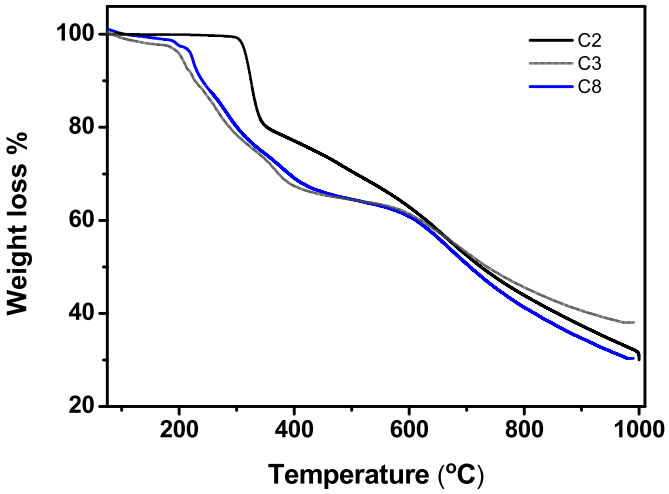

Fig. 5. TGA curves of selected some the complexes ($\mathbf{C_2}$, $\mathbf{C_3}$, $\mathbf{C_8}$).

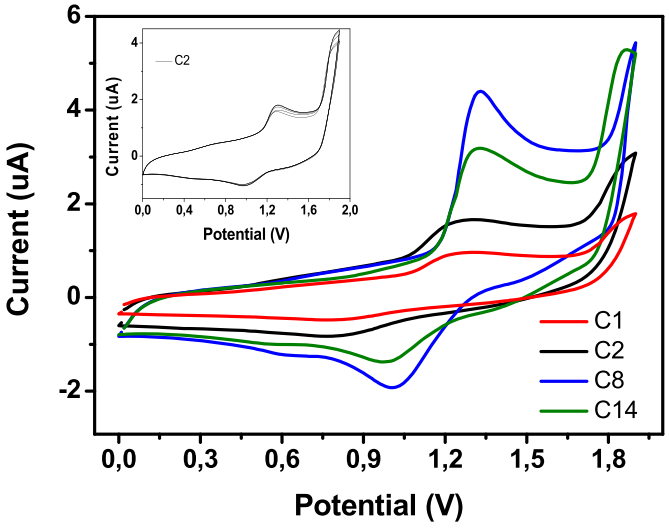

Fig. 6. a) Cyclic voltammograms of the complexes ($\mathbf{C_1}$, $\mathbf{C_2}$, $\mathbf{C_8}$, $\mathbf{C_{14}}$) **b)** 6 consecutive cyclic voltammograms of complex ($\mathbf{C_2}$) measured in CH_3CN solutions with scan speed of 100 mVs^{-1}.

molecular orbital (HOMO) [34]. The oxidation peaks of the complexes ($\mathbf{C_8}$, $\mathbf{C_{14}}$) are slightly shifted to anodic area in the presence of *N*-naphtyl substituent on 2-(2′-quinolyl)benzimidazoles ligands. The HOMO energy levels of the complexes (E_{HOMO}) were determined using the maximum of first oxidation potentials ($E_{HOMO} = -e(E_{1/2(ox.)} - E_{1/2(Fe)} + 4.8)$) [35]. The LUMO energy levels of $\mathbf{C_{1\text{-}14}}$ (E_{LUMO}) were determined from the equation $E_{LUMO} = E_{HOMO} + Eg$ where *Eg* is optical band gap (Eg) [36]. The energy levels of HOMO and LUMO for the complexes are in the range of −5.57 to −5.67 eV and −2.50 to −2.71 eV, respectively. The corresponding data are summarized in Table 5. The consecutive voltammograms were obtained to investigate electrochemical stable of the complexes. In anodic area, there is no an important change in peak currents and potentials (Fig. 6b). This shows the electrochemically stable of molecules.

The computational calculations of E_{HOMO}, E_{LUMO} and band gap of the complexes ($\mathbf{C_1}$ and $\mathbf{C_8}$) were performed in gas phase and data are summarized in Table 6. The HOMO orbitals of complex **1** are delocalized over ruthenium metal and *p*-cymene and LUMO is composed of $\mathbf{L_1}$ ligand. In comparion of the obtained theoretical results, the

Table 5
The electrochemical data of the ruthenium complexes ($\mathbf{C_{1\text{-}14}}$) in CH_3CN.

Complex	E_{ox} (V)	HOMO (eV)	LUMO (eV)	Band Gap (E_g) (eV)
C1	1.24	−5.58	−2.56	3.02
C2	1.23	−5.57	−2.60	2.97
C3	1.26	−5.60	−2.50	3.10
C4	1.27	−5.61	−2.51	3.10
C5	1.27	−5.61	−2.69	2.92
C6	1.27	−5.61	−2.69	2.92
C7	1.28	−5.62	−2.70	2.92
C8	1.33	−5.67	−2.57	3.13
C9	1.25	−5.59	−2.60	2.99
C10	1.26	−5.60	−2.61	2.99
C11	1.26	−5.60	−2.61	2.99
C12	1.26	−5.60	−2.61	2.99
C13	1.27	−5.61	−2.62	2.99
C14	1.32	−5.66	−2.71	2.95

difference between the theoretical (in gas phase) and the experimental data (in solution phase) was observed for complexes 1 and 8 (Fig. 7). The difference of the electrochemical parameters in gas and solution phases may be attributed to an intrinsic resistance of electrolyte solution in the electrochemical cell [37].

3.5. Catalytic studies

The catalytic transfer hydrogenation of acetophenone was investigated by the synthesized half-sandwich Ru^{II} complexes ($\mathbf{C_{1\text{-}14}}$) as catalyst. The catalytic experiments were performed in a 15 mL two-necked round bottomed flask equipped with magnetic stirrer and condenser. All catalytic experiments were tested under identical conditions to allow comparison of results. For this, a typical catalytic reaction were carried out at 82 °C in open air using catalyst, $\mathbf{C_{1\text{-}14}}$ (0.01 mmol), KOH (4 mmol) as co-catalyst, acetophenone (1 mmol) and 2-propanol (4 ml) as a source of hydrogen and solvent, taking into account the pre-determined optimum conditions for transfer hydrogenation with this similar type catalyst, the best ratio of S/C/B [3b]. All catalytic reactions were monitored by GC. The results showed that the catalytic transfer hydrogenation of acetophenone could be obtained with high efficiency for all catalysts ($\mathbf{C_{1\text{-}14}}$). The catalytic results are given in Fig. 8. When the values in the Fig. 8 are examined, the best results were obtained with $\mathbf{C_1}$ and $\mathbf{C_2}$. This inference may be related to NH functionality. However, the presence of methyl groups at the 5,6-positions in the benzimidazole skeleton in the ligand structure (*2-(5,6-dimethyl-1H-benzimidazol*-2-yl)*quinoline*, $\mathbf{L_2}$) in the $\mathbf{C_2}$ complex appears to reduce catalytic activity to some extent. The N-H protons at $\mathbf{C_1}$ and $\mathbf{C_2}$ may play an important role in the transfer hydrogenation mechanism via metal-ligand cooperativity. Namely, at the transition state, hydrogen bonding ability between N-H protons and catalytic species (ketones or IPA) (Fig. 9) may increase catalytic activity compared to $\mathbf{C_2}$-$\mathbf{C_{14}}$ analogs [38]. Looking at other complex series ($\mathbf{C_3}$-$\mathbf{C_7}$ and $\mathbf{C_9}$-$\mathbf{C_{13}}$), the catalytic activity appears to depend not only on the quinolinyl-benzimidazole skeleton of the ligand structures but also on the benzyl fragment of the ligands. Interestingly, the efficiency of the catalyst decreases due to the number of methyl

Table 6
The calculated and experimental electrochemical parameters of the complexes (C_1 and C_8).

Complex	HOMO (eV)		LUMO (eV)		Band Gap (eV)	
	Expt.	Calc.	Expt.	Calc.	Expt.	Calc.
C_1	−5.58	−5.33	−2.56	−3.39	3.02	1.94
C_8	−5.67	−8.57	−2.57	−6.47	3.13	2.10

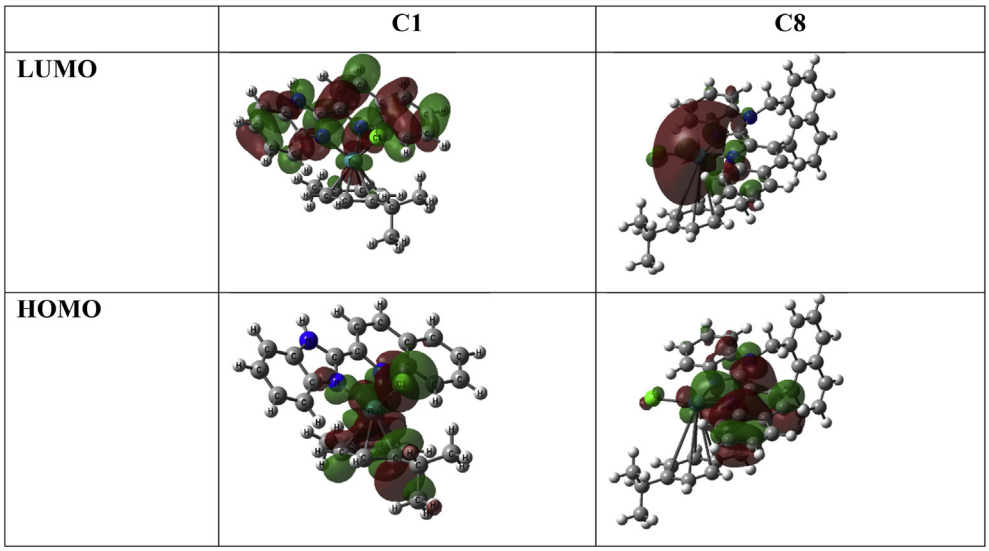

Fig. 7. Frontier orbital electron distribution for the HOMOs and LUMOs of the $\mathbf{C_1}$ and $\mathbf{C_8}$.

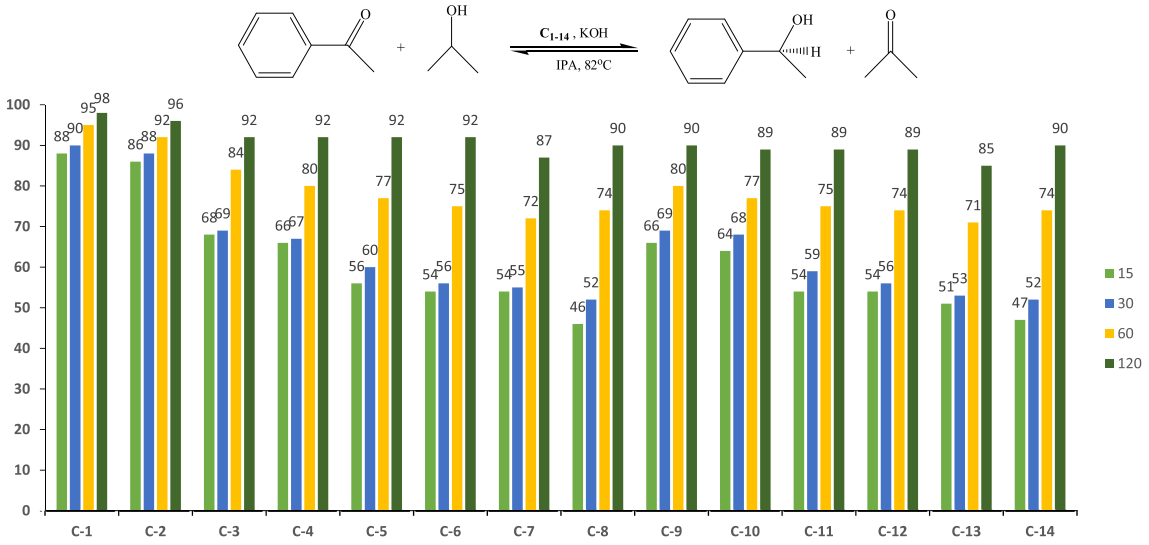

Fig. 8. TH of acetophenone (1.0 mmol) catalyzed by $\mathbf{C_{1\text{-}14}}$ (0.01 mmol) using KOH (4.0 mmol) in the presence of 2-propanol (4.0 mL).

groups as electron donating group in the aromatic ring introduce to the benzyl fragment. $\mathbf{C_8}$ and $\mathbf{C_{14}}$ complexes containing naphtyl group on the nitrogen atom in benzimidazole skeleton in ligand structure showed close activity to each other.

4. Conclusion

In this work, we reported the preparation and characterization of a series of the half-sandwich Ru^{II} complexes, [RuCl($L_{1\text{-}14}$)(η^6-*p*-cymene)]Cl; ($\mathbf{C_{1\text{-}14}}$) with bidentate ligands ($\mathbf{L_{1\text{-}14}}$) containing 2-(2′-quinolyl)benzimidazole derivative and their catalytic activities for hydrogen transfer reaction of acetophenone with the use of 2-propanol in the presence of KOH under open air. Besides, the thermal and electrochemical properties of the selected ruthenium complexes were investigated. Four novel ligand ($\mathbf{L_2}$, $\mathbf{L_4}$, $\mathbf{L_{12}}$ and $\mathbf{L_{14}}$) were structurally characterized with single crystal X-ray diffraction. The catalytic reactions show that $\mathbf{C_1}$ and $\mathbf{C_2}$ are more efficient catalyst than other $\mathbf{C_{3\text{-}14}}$ for TH of acetophenone. Generally, the efficiency of the catalyst seems to depend on the steric and electronic parameters of $\mathbf{L_{3\text{-}14}}$. When ruthenium complexes are compared; depending on the number and positions of the electron

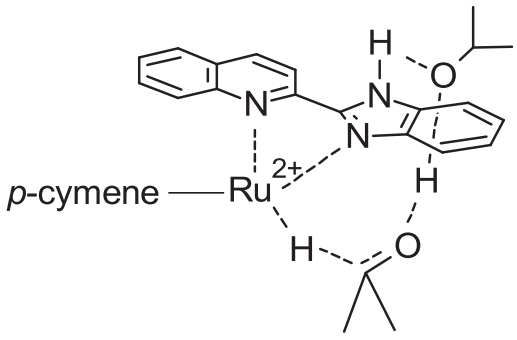

Fig. 9. The proposed transition state of catalytic species.

donor methyl groups on phenyl substituent in the **C_3-C_7** and **C_9-C_{13}** series, besides the presence of methyl groups in the 5,6-positions of the benzimidazole for **C_9-C_{13}** series, decreased the catalytic efficiency. A similar situation was observed when **C_8** and **C_{14}** were compared, and the presence of electron donating methyl groups at the 5,6-positions of the benzimidazole in ligand structure (**C_{14}**) slightly reduced the catalytic yield. The 2-naphtylmethyl, benzyl, methyl group(s) on phenyl substituent effects on the steric and electronic properties of *N,N*-type ligands (**$L_{3\text{-}14}$**) were assessed through experimental involving ruthenium complexes.

Author statement

Ahmet Erdem: Experimentals; Synthesis and Purifications, crystallization. Rafet Kılınçarslan: Experimentals and methodology; Synthesis and Purifications, Writing- Reviewing and Editing, Management organization. Çiğdem Şahin: Cyclic voltammetry, Thermogravimetric measurement and interpretation. Osman Dayan: Experimentals; Synthesis and Purifications and crystallization and interpretation. Namık Özdemir: X-ray diffractions measurements and interpretation

Acknowledgements

We acknowledge Pamukkale University Scientific Research Projects Commission (Project No: 2014FBE035 and 2017FEBE042) and Ondokuz Mayıs University (Project No: PYO.FEN.1906.19.001) for support. Also, we would like to thank Prof. Dr. İzzet Kara (Pamukkale University, Faculty of Education) for his contribution in making theoretical calculations using Gaussian 16 package and Gauss view 6.

Appendix A. Supplementary data

Supplementary data to this article can be found online at https://doi.org/10.1016/j.molstruc.2020.128556.

References

[1] (a) D. Wang, D. Astruc, The golden age of transfer hydrogenation, Chem. Rev. 115 (2015) 6621–6686, https://doi.org/10.1021/acs.chemrev.5b00203;
(b) E. Baráth, Hydrogen transfer reactions of carbonyls, alkynes, and alkenes with noble metals in the presence of alcohols/ethers and amines as hydrogen donors, Catalysts 8 (2018) 671–696, https://doi.org/10.3390/catal8120671.

[2] (a) D. Pandiarajan, R. Ramesh, Ruthenium(II) half-sandwich complexes containing thioamides: synthesis, structures and catalytic transfer hydrogenation of ketones, J. Organomet. Chem. 723 (2013) 26–35, https://doi.org/10.1016/j.jorganchem.2012.10.003;
(b) D. Mercan, E. Çetinkaya, E. Şahin, Ru(II) arene complexes with N-substitued 3,4-dihydroquinazoline ligands and ctalytic activity for transfer hydrojenation reaction, Inorg. Chim. Acta. 400 (2013) 74–81, https://doi.org/10.1016/j.ica.2013.02.005.

[3] (a) S.A. Moya, C.N. Vergara, K. Brown, V. Artigas, M. Fuentealba, V. Guerchais, Transfer hydrogenation of N-benzlideneaniline catalzed by ruthenium complexes with pincer-type phosphorous nitrogen ligands using propan-2-ol as the hydrogen source, Catal. Commun. 99 (2017) 150–153, https://doi.org/10.1016/j.catcom.2017.04.026;
(b) O. Dayan, S. Demirmen, N. Özdemir, Heteroleptic ruthenium(II) complexes of 2-(2-pyridyl)benzimidazoles: a study of catalytic efficiency towards transfer hydrogenation of acetophenone, Polyhedron 85 (2015) 926–932, https://doi.org/10.1016/j.poly.2014.10.012;
(c) L. Wang, Q. Yang, H. Chen, R.X. Li, A novel cationic dinuclear ruthenium complex: synthesis, characterizasyon and catalytic activity in the transfer hydrogenation of ketons, Inorg. Chim. Commun. 14 (2011) 1884–1888, https://doi.org/10.1016/j.inoche.2011.09.003.

[4] D. Klomp, U. Hanefeld, J.A. Peters, Transfer hydrogenation including the Meerwein-Ponndorf-Verley reduction, in: J.G. de Vries, C.J. Elsevier (Eds.), The Handbook of Homogeneous Hydrogenation, first ed., Wileyvch Verlag GmbH & Co. KGaA, Weinheim, Germany, 2007, ISBN 978-3-527-31161-3 (Chapter 20), 585–630.

[5] (a) B. Çetinkaya, B. Alıcı, İ. Özdemir, C. Bruneau, P.H. Dixneuf, 2-imidazoline and 1,4,5,6-tetrahydropyrimidine–ruthenium(II) complexes and catalytic synthesis of furan, J. Organomet. Chem. 575 (1999) 187–192, https://doi.org/10.1016/S0022-328X(98)00992-9;
(b) B. Çetinkaya, İ. Özdemir, C. Bruneau, P.H. Dixneuf, Benzimidazole, benzothiazole and benzoxazole ruthenium(II) complexes; Catalytic synthesis of 2,3-dimethylfuran, Eur. J. Inorg. Chem. 1 (2000) 29–32, https://doi.org/10.1002/(SICI)1099-0682(200001)2000:1<29::AID-EJIC29>3.0.CO;2-M;
(c) J.M. Gichumbi, H.B. Friedrich, Half-sandwich complexes of platinum group metals (Ir, Rh, Ru and Os) and some recent biological and catalytic applications, J. Organomet. Chem. 866 (2018) 123–143, https://doi.org/10.1016/j.jorganchem.2018.04.021.

[6] K.S. Singh, W. Kaminsky, Arene ruthenium(II) azido complexes incorporating N∩O chelate ligands: synthesis, spectral studies and 1,3-dipolar-cycloaddition to a coordinated azide in ruthenium(II) compounds, Polyhedron 68 (2014) 279–286, https://doi.org/10.1016/j.poly.2013.10.032;
(b) W.-G. Jia, H. Zhang, T. Zhang, S. Ling, Synthesis, structure and catalytic activities of half-sandwich ruthenium complexes based on Schiff Base ligands, Inorg. Chem. Commun. 66 (2016) 15–18, https://doi.org/10.1016/j.inoche.2016.02.001;
(c) L. Gök, H. Türkmen, Half-sandwich η6-arene-ruthenium(II) complexes bearing1-alkyl(benzyl)-imidazo[4,5-f][1,10]-phenanthroline (IP) derivatives: the effect of alkyl chain length of ligands to catalytic activity, Tetrahedron 69 (2013) 10669–10674, https://doi.org/10.1016/j.tet.2013.09.023;
(d) İ. Özdemir, N. Şahin, B. Çetinkaya, Transfer hydrogenation of ketones catalyzed by 1-alkylbenzimidazole ruthenium(II) complexes, Monatsh. Chem. 138 (2007) 205–209, https://doi.org/10.1007/s00706-007-0590-9.

[7] a) O. Dayan, M. Tercan, N. Özdemir, Syntheses and molecular structures of novel Ru(II) complexes with bidentate benzimidazole based ligands and their catalytic efficiency for oxidation of benzyl alcohol, J. Mol. Struct. 1123 (2016) 35–43, https://doi.org/10.1016/j.molstruc.2016.06.017;
b) L.T. Ghoochany, S. Farsadpour, Y. Sun, W.R. Thiel, N. New N, N-donors resulting in highly active ruthenium catalysts for transfer hydrogenation at room temperature, Eur. J. Inorg. Chem. (2011) 3431–3437, https://doi.org/10.1002/ejic.201100459.

[8] a) O. Dayan, B. Çetinkaya, Mono- and binuclear ruthenium(II) complexes containing pyridine-2,6-diimine (pydim) ligands: synthesis, characterization and catalytic activity in the transfer hydrogenation of acetophenone, J. Mol. Catal. Chem. 271 (2007) 134–141, https://doi.org/10.1016/j.molcata.2007.02.026;
b) W. Jin, L. Wang, Z. Yu, A highly active ruthenium(II) pyrazolyl-pyridyl-pyrazole complex catalyst for transfer hydrogenation of ketones, Organometallics 31 (2012) 5664–5667, https://doi.org/10.1021/om300602w;
c) F. Zeng, Z. Yu, Exceptionally efficient unsymmetrical ruthenium(II) NNN complex catalysts bearing a pyridyl-based pyrazolyl-imidazolyl ligand for transfer hydrogenation of ketones, Organometallics 27 (2008) 2898–2901, https://doi.org/10.1021/om8002043.

[9] S. Karabuga, S. Bars, İ. Karakaya, S. Gümüs, Efficient transfer hydrogenation reactions with quinazoline-based ruthenium complexes, Tetrahedron Lett. 56 (2015) 101–104, https://doi.org/10.1016/j.tetlet.2014.11.027.

[10] W. Baratta, E. Herdtweck, K. Siega, M. Toniutti, P. Rigo, 2-(Aminomethyl) pyridine-phosphine ruthenium(II) complexes: novel highly active transfer hydrogenation catalysts, Organometallics 24 (2005) 1660–1669, https://doi.org/10.1021/om0491701.

[11] a S. Hashiguchi, A. Fujii, J. Takehara, T. Ikariya, R. Noyori, Asymmetric transfer hydrogenation of aromatic ketones catalyzed by chiral ruthenium(II) complexes, J. Am. Chem. Soc. 117 (1995) 7562–7756, https://doi.org/10.1021/ja00133a037;
b) A. Fujii, S. Hashiguchi, N. Uematsu, T. Ikariya, R. Noyori, Ruthenium(II)-catalyzed asymmetric transfer hydrogenation of ketones using formic acid-triethylamine mixture, J. Am. Chem. Soc. 118 (1996) 2521–2522, https://doi.org/10.1021/ja954126l;
c) J. Takehara, S. Hashiguchi, A. Fujii, S. Inoue, T. Ikariya, R. Noyori, Amino alcohol effects on the ruthenium(II)-catalysed asymmetric transfer hydrogenation of ketones in propan-2-ol, Chem. Commun. (1996) 233–234, https://doi.org/10.1039/CC9960000233.

[12] a) R. Noyori, S. Hashiguchi, Asymmetric transfer hydrogenation catalyzed by chiral ruthenium complexes, Acc. Chem. Res. 30 (1997) 97–102, https://doi.org/10.1021/ar9502341;
b) S. Gladiali, E. Alberico, Asymmetric transfer hydrogenation: chiral ligands and applications, Chem. Soc. Rev. 35 (2006) 226–236, https://doi.org/10.1039/B513396C;
c) T. Ikariya, A.J. Blacker, Asymmetric transfer hydrogenation of ketones with bifunctional transition metal-based molecular catalysis, Acc. Chem. Res. 40 (2007) 1300–1308, https://doi.org/10.1021/ar700134q.

[13] J.G. Malecki, A. Maron, S. Krompiec, M. Filapek, M. Penkala, B. Marcol, Synthesis, characterizations and catalytic applications of hydridecarbonyl ruthenium(II) complexes with imidazole carboxylic acid derivative ligands, Polyhedron 49 (2013) 190–199, https://doi.org/10.1016/j.poly.2012.09.051.

[14] (a) B. Cornils, W.A. Herrmann, Aqueous-Phase Organometallic Catalysis, second ed., Wiley-VCH, 2002;
(b) W.A. Herrmann, C.W. Kohlpaintner, Water-soluble ligands, metal complexes, and catalysts: synergism of homogeneous and heterogeneous catalysis, Angew. Chem. Int. Ed. 32 (1993) 1524–1544, https://doi.org/10.1002/anie.199315241;
(c) U.M. Lindstrom, Stereoselective organic reactions in water, Chem. Rev. 102 (2002) 2751–2772, https://doi.org/10.1021/cr010122p.

[15] (a) H. Türkmen, İ. Kani, B. Çetinkaya, Transfer hydrogenation of aryl ketones

with half-sandwich Ru^{II} complexes that contain chelating diamines, Eur. J. Inorg. Chem. (2012) 4494–4499, https://doi.org/10.1002/ejic.201200638;
(b) O. Kohle, S. Ruile, M. Grätzel, Ruthenium(II) charge-transfer sensitizers containing 4,4′-dicarboxy-2,2′-bipyridine. Synthesis, properties, and bonding mode of coordinated thio- and selenocyanates, Inorg. Chem. 35 (1996) 4779–4787, https://doi.org/10.1021/ic9515665;
(c) M.K. Nazeeruddin, E. Muller, R. Humphry-Baker, N. Vlachopoulos, M. Grätzel, Redox regulation in ruthenium(II) polypyridyl complexes and their application in solar energy conversion, J. Chem. Soc., Dalton Trans. (1997) 4571–4578, https://doi.org/10.1039/A704242F;
(d) Y. Himeda, N. Onozawa-Komatsuzaki, H. Sugihara, H. Arakawa, K. Kasuga, Transfer hydrogenation of a variety of ketones catalyzed by rhodium complexes in aqueous and their application to asymmetric reduction using chiral Schiff base ligands, J. Mol. Catal. Chem. 195 (2003) 95–100, https://doi.org/10.1016/S1381-1169(02)00576-9;
(e) C. Sahin, M. Ulusoy, C. Zafer, C. Özsoy, C. Varlıklı, T. Dittrich, B. Çetinkaya, S. İcli, The synthesis and characterization of 2-(2′-pyridyl)benzimidazole heteroleptic ruthenium complex: efficient sensitizer for molecular photovoltaics, Dyes Pigments 84 (2010) 88–94, https://doi.org/10.1016/j.dyepig.2009.06.016.

[16] (a) C.P. Casey, G.A. Bikzhanova, Q. Cui, I.A. Guzei, Reduction o imines by hydroxycyclopentadenyl ruthenium hydride: intramolecular trapping evidence for hydride and proton transfer outside the coordination sphere of the metal, J. Am. Chem. Soc. 127 (2005) 14062–14071, https://doi.org/10.1021/ja053956o;
(b) A. Zanotti-Gerosa, W. Hems, M. Groarke, F. Hancock, Ruthenium-catalysed asymmetric reduction of ketones, Platin. Met. Rev. 49 (2005) 158–165, https://doi.org/10.1595/147106705X75421;
(c) J. Soleimannejad, A. Sisson, C. White, Functionalized-arene ruthenium half-sandwich compounds as enantioselective hydrogen transfer catalysts. Crystal structures of $[RuCl\{TsNCH(R)CH(R)NH_2\}(\eta^6\text{-}C_6H_5OCH_2CH_2OH)]$ (R = H or Ph), Inorg. Chim. Acta. 352 (2003) 121–128, https://doi.org/10.1016/S0020-1693(03)00151-8;
(d) A.J. Davenport, D.L. Davies, J. Fawcett, D.R. Russell, Arene-ruthenium complexes with salicyloxazolines: diastereoselective synthesis, configurational stability and applications as asymmetric catalysts for Diels-Alder reactions, Dalton Trans. (2004) 1481–1492, https://doi.org/10.1039/B400747F.

[17] a) L.W. Deady, T. Rodemann, G.J. Finlay, B.C. Baguley, W.A. Denny, Synthesis and cytotoxic activity of carboxamide derivatives of benzimidazo [2,1-a]isoquinoline and pyrido[3′,2′:4,5]imidazo[2,1-a]isoquinoline, Anti-Cancer Drug Des. https://www.ingentaconnect.com/contentone/cog/antcan/2000/00000015/00000005/art00005, 2000, 15-339-346;
(b) S.M. Rida, S.A.M. El-Hawash, H.T.Y. Fahmy, A.A. Hazzaa, M.M.M. El-Meligy, Synthesis of novel benzofuran and related benzimidazole derivatives for evaluation of in vitro anti-HIV-1, anticancer and antimicrobial activities, Arch Pharm. Res. (Seoul) 29 (2006) 826–833, https://doi.org/10.1007/BF02973901;
c) V.K. Pandey, A. Shukla, Synthesis and biological activity of isoquinolinyl benzimidazoles, Indian J. Chem. 38 (1999) 1381–1383. http://hdl.handle.net/123456789/16670;
(d) R.L. Weinkauf, A.Y. Chen, C. Yu, L. Liu, L. Barrows, E.J. LaVoie, Antineoplastic activity of benzimidazo[1,2-b]-isoquinolines, indolo[2,3-b]quinolines, and pyridocarbazoles, Bioorg. Med. Chem. 2 (1994) 781–786, https://doi.org/10.1016/s0968-0896(00)82177-x.

[18] a) O. Dayan, N. Özdemir, Z. Şerbetçi, M. Dinçer, B. Çetinkaya, O. Büyükgüngör, Synthesis and catalytic activity of ruthenium(II) complexes containing pyridine-based tridentate triamines ('NNN') and pyridine carboxylate ligands (NO), Inorg. Chim. Acta. 392 (2012) 246–253, https://doi.org/10.1016/j.ica.2012.02.034;
(b) O. Dayan, S. Dayan, I. Kani, B. Çetinkaya, Ruthenium(II) complexes bearing pyridine-based tridentate and bidentate ligands: catalytic activity for transfer hydrogenation of aryl ketones, Appl. Organomet. 26 (2012) 663–670, https://doi.org/10.1002/aoc.2901;
(c) A.K. Vannucci, J.F. Hull, Z. Chen, R.A. Binstead, J.J. Conception, T.J. Meyer, Water oxidation intermediates applied to catalysis: benzyl alcohol oxidation, J. Am. Chem. Soc. 134 (2012) 3972–3975, https://doi.org/10.1021/ja210718u;
(d) J. Diez, J. Gimeno, A. Lledos, F.J. Suarez, C. Vicent, Imıdazole based ruthenium(IV) complexes as highly efficient bifunctional catalysts for the redox isomerization of allylic alcohols in aqueous medium: water as cooperating ligand, ACS Catal. 2 (2012) 2087–2099, https://doi.org/10.1021/cs300369;
(e) W.J. Ye, M. Zhao, W.M. Du, Q.B. Jiang, K.K. Wu, P. Wu, Z.K. Yu, Highly active ruthenium(II) complex catalysts bearing an unsymmetrical NNN ligand in the (asymmetric) transfer hydrogenation of ketones, Chem. Eur J. 17 (2011) 4737–4741, https://doi.org/10.1002/chem.201002039.

[19] a) J. Zhou, S. Zhi, H. Yu, R. Mao, J. Hu, W. Song, J. Zhang, Mitochondrial and nuclear DNA dual damage induced by 2-(2′-quinoly)benzimidazole copper complexes with potential anticancer activity, RSC Adv. 7 (2017) 51162–51174, https://doi.org/10.1039/c7ra09102h;
b) J. Zhou, Z.G. Lu, G.G. Shan, S.H. Wang, Y. Liao, Gadolinium complex and phosphorescent probe-modified NaDyF4 nanorods for T-1- and T-2-weighted MRI/CT/phosphorescence multimodality imaging, Biomaterials 35 (2014) 368–377, https://doi.org/10.1016/j.biomaterials.2013.09.088;
(c) W.J. Zhang, W. Huang, T.L. Liang, W.H. Sun, Half-Titanocene chlorides 2-(benzimidazol-2-yl)quinoline-8-olates: synthesis, characterization and ethylene (co-)polymerization behavior, Chin. J. Polym. Sci. 31 (2013) 601–609, https://doi.org/10.1007/s10118-013-1253-4;
(d) S. Li, B. Zhang, F.E. Kuhn, Benzimidazolic complexes of methyltrioxorhenium(VII): synthesis and application in catalytic olefin epoxidation, J. Organomet. Chem. 730 (2013) 132–136, https://doi.org/10.1016/j.jorganchem.2012.11.006;
(e) J.J. Xia, Z.H. Zhou, W. Li, H.Q. Zhang, C. Redshaw, W.H. Sun, Synthesis, structure and fluorescent properties of 2-(1H-benzoimidazol-2-yl)quinoline-8-ol ligands and their zinc complexes, Inorg. Chim. Acta. 394 (2013) 569–575, https://doi.org/10.1016/j.ica.2012.09.012;
(f) F. He, X. Hao, X.P. Cao, C. Redshaw, W.H. Sun, Nickel halide complexes bearing 2-benzimidazolyl-N-aryquinoline-8-carboxamide derived ligands: synthesis, characterization and catalytic behavior towards ethylene oligomerization and the vinyl polymerization of norbornene, J. Organomet. Chem. 712 (2012) 46–51, https://doi.org/10.1016/j.organchem.2012.04.013;
(g) J.H. Min, Q.S. Zhang, W. Sun, Y.X. Cheng, L.X. Wang, Neutral copper(I) phosphorescent complexes from their ionic counterparts with 2-(2′-quinolyl) benzimidazole and phosphine mixed ligands, Dalton Trans. 40 (2011) 686–693, https://doi.org/10.1039/c0dt01031f;
(h) S.J. Li, Y. Li, Synthesis and properties of a novel ruthenium complex containing a 2-(benzimidazol-2yl)-8-octyloxyquinoline tridentate ligand, Inorg. Chem. Commun. 14 (2011) 683–685, https://doi.org/10.1016/j.inoche.2011.02.005;
(i) L. He, J. Qiao, L. Duan, G.F. Dong, D.Q. Zhang, L.D. Wang, Y. Qiu, Toward highly efficient solid-state white light-emitting electrochemical cells: blue-green to red emitting cationic iridium complexes with imidazole-type ancillary ligands, Adv. Funct. Mater. 19 (2009) 2950–2960, https://doi.org/10.1002/adfm.200900723;
(j) A.J. Hallett, B.D. Ward, B.M. Kariuki, S.J.A. Pope, Neutral and cationic cyclometallated Ir(III) complexes of anthra[1,2-d]-imidazole-6,11-dione-derived ligands: syntheses, structures and spectroscopic characterisation, J. Organomet. Chem. 695 (2010) 2401–2409, https://doi.org/10.1016/j.jorganchem.2010.07.017;
(k) Z.C. Zhu, M. Kojima, K. Nakajima, Reversible ring opening and closure reactions of the triazine ligands derived from 1-phenylazo-2-naphthylamine and pyridine-2-aldehyde or quinoline-2-aldehyde structure and reactivity of the palladium(II) complexes, Inorg. Chim. Acta. 358 (2005) 476–488, https://doi.org/10.1016/j.ica.2004.08.024;
(l) F.A. Sahki, L. Messaadia, H. Merazig, A. Chiabani, A. Bouraiou, S. Bouacida, Synthesis, x-ray structure and theoretical investigation of 2-(2′-quinolyl) benzimidazole metal complexes, J. Chem. Sci. 129 (2017) 21–29, https://doi.org/10.1007/s12039-016-1210-1.

[20] a) T.R. Chen, Synthesis, structure, and field-effect property of 2-(benzimidazol-2yl) quinoline, Mater. Lett. 59 (2005) 1050–1052, https://doi.org/10.1016/j.matlet.2004.12.002;
b) M.A. Bennett, T.N. Huang, T.W. Matheson, A.K. Simith, Eta-5-hexamethylbenzene)ruthenium complexes, Inorg. Synth. 21 (1982) 74–78, https://doi.org/10.1002/9780470132524.ch16.

[21] a) W.K. Huang, C.W. Cheng, S.M.S.M. Chang, Y.P. Lee, E.W.G. Diau, Synthesis and electron-transfer properties of benzimidazole-functionalized ruthenium complexes for highly efficient dye-sensitized solar cells, Chem. Commun. 46 (2010) 8992–8994, https://doi.org/10.1039/c0cc03517c;
b) N.M. Shavaleev, Z.R. Bell, T.L. Easun, R. Rutkaite, L. Swanson, M.D. Ward, Complexes of substituted derivatives of 2-(2-pyridyl)benzimidazole with Re(I), Ru(II) and Pt(II): structures, redox and luminescence properties, Dalton Trans. (2004) 3678–3688, https://doi.org/10.1039/b411341a.

[22] Stoe & Cie, X-AREA Version 1.18 and X-RED32 Version 1.04, Stoe & Cie, Darmstadt, Germany, 2002.

[23] M.C. Burla, R. Caliandro, B. Carrozzini, G.L. Cascarano, C. Cuocci, C. Giacovazzo, M. Mallamo, A. Mazzone, G. Polidori, Crystal structure determination and refinement via SIR2014, J. Appl. Crystallogr. 48 (2015) 306–309, https://doi.org/10.1107/S1600576715001132.

[24] G.M. Sheldrick, Crystal structure refinement with SHELXL, Acta Crystallogr. C 71 (2015) 3–8, https://doi.org/10.1107/S2053229614024218.

[25] O.V. Dolomanov, L.J. Bourhis, R.J. Gildea, J.A.K. Howard, H. Puschmann, OLEX2: a complete structure solution, refinement and analysis program, J. Appl. Crystallogr. 42 (2009) 339–341, https://doi.org/10.1107/S0021889808042726.

[26] V.A. Mamedov, D.F. Saifina, A.T. Gubaidullin, V.R. Ganieva, S.F. Kadyrova, D.V. Rakov, I.K. Rizvanov, O.G. Sinyashin, Acid-catalyzed rearrangement of 3-(beta-2-aminostyryl)quinoxalin-2(1H)ones-a-new and efficient method for the synthesis of 2-benzimidazol-2-ylquinolines, Tetrahedron Lett. 51 (2010) 6503–6506, https://doi.org/10.1106/j.tetlet.2010.10.007.

[27] F.H. Allen, O. Kennard, D.G. Watson, L. Brammer, O.A.G.R. Taylor, Tables of bond lengths determined by x-ray and neutron-diffraction. 1.bond lengths in organic compounds, J. Chem. Soc. Perkin Trans. 2 (1987) 1–19, https://doi.org/10.1039/p298700000s1.

[28] T.-R. Chen, A. Yeah, J.-D. Chen, A new imidazolylquinoline for organic thin film transistor, Tetrahedron Lett. 46 (2005) 1569–1571, https://doi.org/10.1016/j.tetlet.2004.12.139.

[29] E. Terazzi, L. Guenee, B. Bocquet, J.-F. Lemonnier, N.D. Favera, C. Piguet, A simple chemical tuning of the effective concentration: selection of single-, double-, and triple-stranded binuclear lanthanide helicates, Chem. Eur J. 15 (2009) 12719–12732, https://doi.org/10.1002/chem.200902026.

[30] S.J. Kim, E.T. Kool, Sensing metal ions with DNA building blocks: fluorescent pyridobenzimidazole nucleosides, J. Am. Chem. Soc. 128 (2006) 6164–6171, https://doi.org/10.1021/ja0581806.

[31] N.M. Shavaleev, R. Scopelliti, F. Gumy, J.-C.G. Bünzli, Near-infrared luminescence of nine-coordinate neodymium complexes with benzimidazole-substituted 8-hydroxyquinolines, Inorg. Chem. 47 (2008) 9055–9068, https://doi.org/10.1021/jc8010585.
[32] K. Wang, M. Shen, W.-H. Sun, Synthesis, characterization and ethylene oligomerization of nickel complexes bearing N-(2-(1H-benzo[d]imidazol-2-yl) quinoline-8-yl)benzamide derivatives, Dalton Trans. (2009) 4085–4095, https://doi.org/10.1039/b822441b.
[33] J. Bernstein, R.E. Davis, L. Shimoni, N.L. Chang, Patterns in hydrogen bonding-functionality and graph set analysis in crystals, Angew. Chem. Int. Ed. 34 (1995) 1555–1573, https://doi.org/10.1002/anie.199515551.
[34] C. Pettinari, F. Marchetti, A. Cerquetella, R. Pettinari, M. Monari, Tatiana C.O. Mac Leod, M.D. Luisa, R.S. Martins, Armando J.L. Pombeiro, Coordination chemistry of the (eta(6)-p-cymene)ruthenium(II) fragment with bis-, tris-, and tetrakis(pyrazol-1-yl)borate ligands: synthesis, structural, electrochemical, and catalytic diastereoselective nitroaldol reaction studies, Organometallics 30 (2011) 1616–1626, https://doi.org/10.1021/om101146q.
[35] B.S. Kim, S.H. Kim, Y.S. Kim, S.H. Kim, Y.A. Son, Synthesis and characterization of quinoline-based dye sensor, Mol. Cryst. Liq. Cryst. 504 (2009) 173–180, https://doi.org/10.1080/00273170902950014.
[36] M. Lin, D. Li, X. Wang, C. Luo, Q. Ling, Synthesis and optical properties of white phosphorescent carbazole-iridium copolymers, J. Macromol. Sci., Pure Appl. Chem. 53 (2016) 222–226, https://doi.org/10.1080/10601325.2016.1143317.
[37] a) N. Elgrishi, K.J. Rountree, B.D. McCarthy, E.S. Rountree, T.T. Eisenhart, J.L. Dempsey, A practical beginner's guide to cyclic voltammetry, J. Chem. Educ. 95 (2018) 197–206, https://doi.org/10.1021/acs.jchemed.7b00361;
b) Electrocatalysis, in: Computational, Experimental, and Industrial Aspects, Carlos Fernando Zinola, CRC press, 2010.
[38] I. Demianets, V. Cherepakhin, A. Maertens, P.J. Lauridsen, S. Mallikarjun Sharada, T.J. Williams, A new mechanism of metal-ligand cooperative catalysis in transfer hydrogenation of ketones, Polyhedron 182 (2020) 114508, https://doi.org/10.1016/j.poly.2020.114508.